Impurity effects in dendritic solidification

Alain Karma and J. S. Langer
Institute for Theoretical Physics, University of California, Santa Barbara, California 93106
(Received 30 July 1984)

We have performed a quantitative calculation of growth rates and tip radii for dendrites growing in undercooled dilute solutions. Included in our calculations are the capillary corrections to the steady-state Ivantsov needle-crystal solutions. Our results show good agreement with available experimental data and support the validity of the marginal-stability theory of dendritic growth.

I. INTRODUCTION

A stability theory of dendritic crystal growth recently has achieved some success in explaining solidification rates in undercooled samples of pure fluids.[1,2] The theory is based on the dynamical hypothesis that the natural operating point of this nonlinear dissipative system lies at or near its point of marginal stability against deformations of the leading tip of the dendrite. Some progress is being made currently in developing a mathematical basis for this conjecture,[3,4] but its validity is still far from clear.

A sharp experimental test of some general aspects of the stability hypothesis can be made by looking at dendritic growth in the presence of dilute impurities.[5] The point here is that chemical diffusivities are generally two or more orders of magnitude smaller than thermal. Thus, because the impurities rejected by an advancing solidification front must diffuse away from this front to permit further growth, it might be assumed that the presence of impurities would decrease growth rates. The stability hypothesis leads to just the opposite conclusion. Their small chemical diffusivity causes the impurities to form a relatively thin boundary layer in front of the solid. This thinner-than-thermal boundary layer causes the liquid-solid interface to be unstable at shorter length scales, and this instability, in turn, leads to sharper, faster dendritic structures. Effects of this kind have been seen experimentally for many years,[6,7] but only very recently has there been a carefully controlled investigation of this phenomenon.[8]

The purpose of this paper is to present a quantitative theory of this impurity effect. (A first version of this theory was published in Ref. 5.) Unfortunately, it turns out to be very difficult, even within the framework of the marginal-stability hypothesis, to carry out an exact calculation. We shall therefore have to make a number of approximations whose validity is not well understood.

(1) We assume that the steady-state growth forms whose stability is to be examined are time-independent, shape-preserving solutions of the thermal and chemical diffusion equations subject to thermodynamic boundary conditions at the solid-liquid interface. Recent theoretical developments[4] indicate that such solutions may not, in fact, exist.

(2) We further assume that these steady-state solutions, in the presence of finite capillarity, are given reasonably accurately by an approximation of the kind first used for pure substances by Temkin[9] and developed in more detail by Kotler and Tarshis,[10] and Trivedi.[11] This is the approximation in which the steady-state shape of the dendritic tip is assumed to be a paraboloid of revolution, the Gibbs-Thomson condition is imposed everywhere, but heat conservation is imposed only at the tip. This kind of approximation appears to be more accurate than the alternative in which the Gibbs-Thomson condition is relaxed,[12] especially for our case in which both thermal and chemical fields must be considered. The choice of steady-state approximation is not very important in most purely thermal situations, where it turns out that the isothermal Ivantsov solutions are adequate. When impurities are added, however, the sharper curvatures that they induce make capillarity relatively more important and both the existence of steady-state solutions and the validity of approximation schemes become seriously questionable.

(3) Probably the most serious of our theoretical compromises is our use of a spherical approximation[2,5] for performing the stability calculation. The full stability problem is extremely difficult even for the purely thermal situation, where it has not yet been carried out quite satisfactorily. Rather than embark on a major computational project for the impurity case, we have resorted to the device of approximating the tip of the dendrite by a sphere which is growing radially at the dendritic tip velocity. Given spherical symmetry, the stability spectrum can be obtained easily by the methods of Mullins and Sekerka.[13] This technique seems to give reasonable agreement with experiment for purely thermal dendrites despite the fact that it produces a very poor approximation to the stability spectrum in a relatively tractable two-dimensional analog.[14] In three dimensions, agreement with experiment requires choosing a new parameter which may, with somewhat dubious justification, be identified as the order of spherical harmonic whose symmetry is most favored by the crystalline anisotropy. In what follows, we shall assume that this approximation continues to make sense, with the same value of the anisotropy parameter, under conditions in which impurity effects are important.

(4) Finally, we continue to make a number of technical approximations which have been made in previous theories and which seem to be of secondary importance. See especially the discussion preceding Eq. (3.18). We do not include crystalline anisotropy except via the anisotro-

py parameter mentioned above. We neglect convective effects in the fluid. In fact, the latter effects do turn out to be important in our analysis of the experimental data and we shall return to this question in Sec. V.

Despite all of the above deficiencies, our theory does produce a good fit to existing experimental data, especially for the initial rise of the dendritic growth velocity as a function of impurity concentration. This fit is obtained without adjustable parameters, and discrepancies appear to be explicable as convection effects. We believe that this agreement is the firmest evidence to date for the basic validity of the stability theory of dendritic growth.

II. STABILITY THEORY FOR PURE SUBSTANCES

In this section the stability theory of dendritic growth is reviewed briefly. In the pure thermal case, the dendritic growth of a solid in an undercooled melt is governed by the rate at which the latent heat generated at the liquid-solid boundary can be conducted away from the interface. The temperature at the interface differs from the melting temperature and is given by the Gibbs-Thomson relation

$$T_M - T_\infty = T_M \left[1 - \frac{\gamma K}{L} \right] , \tag{2.1}$$

where K is the interface curvature, L is the latent heat per unit volume, and γ is the solid-liquid surface tension. The growth of the dendritic system is controlled by the undercooling of the melt, $T_M - T_\infty$, where T_M is the melting temperature and T_∞ is the temperature in the liquid far from the solidification boundary. One usually defines a dimensionless undercooling Δ

$$\Delta = \frac{T_M - T_\infty}{L/c_p} ,$$

where c_p is the specific heat per unit volume. Similarly, a dimensionless tip radius $\tilde{\rho}$ and growth velocity V can be written as

$$\tilde{\rho} = \rho / d_0$$

and

$$V = v d_0 / 2\alpha ,$$

where d_0 is the capillary length

$$d_0 = T_M \gamma c_p / L^2 ,$$

α is the thermal diffusion constant for the liquid, and ρ and v are the actual tip radius and tip velocity of the dendrite. The whole problem of mode selection is now to predict which tip radius and growth velocity the dendritic system will choose at a given undercooling. This question of mode selection for the dendrite can be answered in two steps. First we determine the family of possible steady-state forms of growth, the so-called "needle crystals," by solving a heat-flow problem in which the moving interface is a heat source, and next we look at the stability of the needle tip and determine the uniquely selected member of the family of growth rates by identifying the point of marginal stability.

If we assume that the tip radius is sufficiently large compared to d_0 that we can neglect capillary corrections and assume the interface to be isothermal, the heat-flow problem is exactly soluble. (We shall discuss approximate corrections to the isothermal limit in Sec. III.) The steady-state motion of the dendrite is given by the Ivantsov solution for an isothermal, cylindrically symmetric, paraboloidal needle crystal. The result of interest here is

$$\Delta = p_L e^{p_L} \mathrm{E}_1(p_L) , \tag{2.2}$$

where $\mathrm{E}_1(p_L)$ is the standard exponential function

$$\mathrm{E}_1(p_L) = \int_{p_L}^{\infty} \frac{e^{-y}}{y} dy \tag{2.3}$$

and p_L is the thermal Péclet number

$$p_L = \frac{\rho v}{2\alpha} = \tilde{\rho} V .$$

Note that $p_L \equiv p_L(\Delta)$ is uniquely determined for a given undercooling Δ and that consequently we have a family of allowed steady-state forms of growth where for a given state the growth speed is inversely proportional to the tip radius.

In order to obtain a second relation between tip radius and growth speed we now look at the stability of the tip. In particular, we define a dimensionless stability parameter

$$\sigma = \left[\frac{\lambda_s}{2\pi\rho} \right]^2 , \tag{2.4}$$

where λ_s is the stability length

$$\lambda_s = 2\pi \sqrt{2\alpha d_0 / v} . \tag{2.5}$$

The parameter σ can also be written as

$$\sigma = \frac{1}{\tilde{\rho}^2 V} = \frac{1}{\tilde{\rho} p_L(\Delta)} . \tag{2.6}$$

A stability analysis of the tip of the dendrite shows that capillary forces stabilize the tip whenever σ exceeds some critical value σ^*. Consequently, for a given undercooling Δ, it follows from Eq. (2.6) that only dendrites which have a tip radius smaller than $1/\sigma^* p_L(\Delta)$ will grow stably. At this stage it is clear that the linear-stability analysis of the tip allows us to restrict the family of steady-state growth forms $[\tilde{\rho} < 1/\sigma^* p_L(\Delta)]$, but has not succeeded in selecting a single mode of growth. To carry the analysis further one conjectures that the nonlinear sidebranching activity near the tip drives the dendrite to a natural operating mode at or near the point of marginal stability ($\sigma = \sigma^*$). The growth speed and tip radius are now uniquely determined for a given undercooling Δ:

$$V(\Delta) = \sigma^* [p_L(\Delta)]^2 , \tag{2.7}$$

$$\tilde{\rho}(\Delta) = \frac{1}{\sigma^* p_L(\Delta)} . \tag{2.8}$$

The simplest way to evaluate σ^* analytically is to approximate the tip of the dendrite by a solid sphere of radius ρ growing at radial velocity v in an undercooled melt. The analysis for the growing sphere has been described in

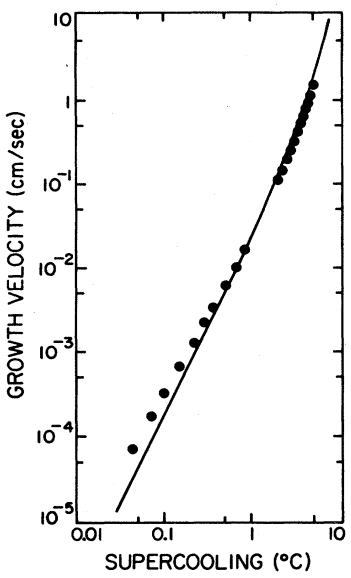

FIG. 1. Growth velocity vs supercooling for pure succinonitrile. Solid line shows the results of the stability theory, and the experimental results of Glicksman, Schaefer, and Ayers (Ref. 15) and Huang and Glicksman (Ref. 16) are indicated by circles.

one of the original papers by Mullins and Sekerka.[13] They use a quasistationary approximation and find that a deformation proportional to the spherical harmonic of order l will grow with an amplification rate ω_l, where

$$\omega_l=\frac{v(l-1)}{\rho}\left[1-\frac{2\alpha d_0}{\rho^2 v}\frac{(l+1)(l+2)}{2}\times\left[1+\frac{l\alpha' c_p'}{(l+1)\alpha c_p}\right]\right]. \tag{2.9}$$

Here, the primed quantities refer to properties of the solid phase, unprimed to the liquid. At the point of marginal stability, $\sigma=\sigma^*$, a perturbation of the tip neither grows nor decays, $\omega_l=0$, and therefore we obtain

$$\frac{1}{\sigma^*}=\tfrac{1}{2}(l+1)(l+2)\left[1+\frac{l\alpha' c_p'}{(l+1)\alpha c_p}\right]. \tag{2.10}$$

For succinonitrile with the choice $l=6$ corresponding to cubic symmetry, and $\alpha' c_p' \cong \alpha c_p$, we have $\sigma^* \cong 0.0192$. Combining the above value of σ^* with the expressions for the dimensionless growth speed and tip radius in Eqs. (2.7) and (2.8), we obtain a quantitative prediction of the selected mode of growth at a given undercooling. A comparison between theory and experiment is shown for the growth velocity as a function of undercooling in Fig. 1.

III. STEADY-STATE THEORY WITH IMPURITIES

We now turn to a situation where a small amount of impurities is added to the undercooled melt. For a given temperature of the solid-liquid interface, the concentration of impurities is usually much greater in the melt than in the solid. As a result of this discontinuity in solute concentration there will be a buildup of impurities in front of the interface which is analogous to the latent heat in the case of thermal diffusion. The growth of the dendritic system is therefore governed by both heat diffusion and chemical diffusion away from the interface. In order to determine the selected tip radius and growth velocity we apply the same techniques used in Sec. II for the pure thermal case. First we solve a coupled heat-flow and chemical diffusion problem in which the moving paraboloidal tip is a source of both latent heat and impurities, and next we perform a stability analysis of the tip in the spherical approximation and determine the point of marginal stability. We now turn to the first part of this calculation.

Let us consider a two-component system for which the phase diagram has the form shown in Fig. 2. For simplicity we assume zero solubility of impurities in the solid. We work in parabolic coordinates (see Fig. 3), $\xi=(r-z)/\rho$ and $\eta=(r+z)/\rho$, where r is the radial distance from the origin 0 and ρ is the radius of curvature at the tip of the paraboloidal interface. The interface is a paraboloid of revolution (about the z axis) at $\eta=1$. The chemical field in the liquid and the thermal fields are represented by $C(\eta,\xi)$ and $T_i(\eta,\xi)$, respectively, $i=L,S$ where L and S correspond to the liquid and the solid, respectively. It is also convenient to define the dimensionless temperature field

$$U_i(\eta,\xi)=\frac{T_i(\eta,\xi)-T_\infty}{L/c_p},\quad i=L,S\ .$$

The steady-state thermal and chemical fields obey diffusion equations in a frame moving at velocity v with the dendrite

$$\left[\eta\frac{\partial^2}{\partial\eta_2}+(1+\eta p)\frac{\partial}{\partial\eta}+\xi\frac{\partial^2}{\partial\xi^2}+(1-\xi p)\frac{\partial}{\partial\xi}\right]\Xi(\eta,\xi)=0\ , \tag{3.1}$$

where $\Xi(\eta,\xi)$ denotes either $C(\eta,\xi)$ or $U_i(\eta,\xi)$, $i=L,S$ and the p's are Péclet numbers:

$$p_L=\rho v/2\alpha\ ,$$

thermal field in the liquid;

$$p_S=\rho v/2\alpha'\ ,$$

thermal field in the solid; and

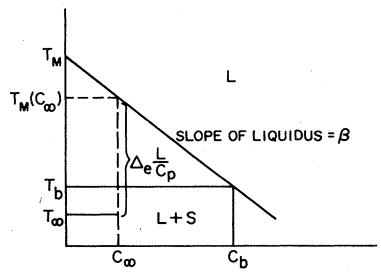

FIG. 2. Schematic phase diagram for dilute solutions. T_b and C_b are the interface temperature and solute concentration, respectively. T_∞ and C_∞ are the temperature and solute concentration far from the interface; Δ_e is the effective undercooling for a solute concentration C_∞.

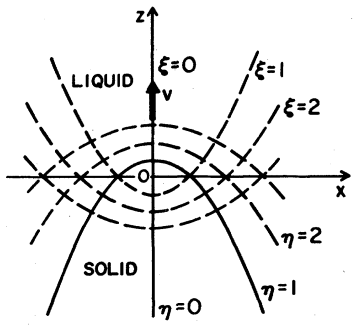

FIG. 3. Parabolic coordinate system.

$$p_C=\rho v/2D\ ,$$

chemical field.

Here, D is the diffusion constant of impurities in the liquid. These diffusion fields are subject to four boundary conditions at the interface.

(1) The Gibbs-Thomson relation couples the thermal and chemical fields at the interface

$$U(1,\xi)+\beta[C(1,\xi)-C_\infty] =\Delta_e-(d_0/\rho)[(2+\xi)/(1+\xi)^{3/2}]\ , \quad (3.2)$$

where d_0 is the capillary length, Δ_e is the effective undercooling for a solution of concentration C_∞, β is the slope of the liquidus, and the ξ-dependent term in brackets is the curvature of the paraboloidal interface.

(2) The temperature is continuous across the interface:

$$U_S(1,\xi)=U_L(1,\xi)\ . \quad (3.3)$$

(3) Heat is conserved at the interface:

$$p_L=\beta^T\frac{\partial U_S}{\partial\eta}\bigg|_{\eta=1}-\frac{\partial U_L}{\partial\eta}\bigg|_{\eta=1}\ , \quad (3.4)$$

where $\beta^T=\alpha' c_p'/\alpha c_p$.

(4) Impurities are conserved at the interface:

$$p_C C(1,\xi)=-\frac{\partial C}{\partial\eta}\bigg|_{\eta=1}\ . \quad (3.5)$$

When capillary forces are neglected ($d_0=0$), we simply recover the steady-state Ivantsov solutions

$$U_L(\eta,\xi)=U_L^0(\eta)=\frac{(T_b-T_\infty)E_1(p_L\eta)}{(L/c_p)E_1(p_L)}\ , \quad (3.6)$$

$$U_S(\eta,\xi)=U_S^0=\frac{T_b-T_\infty}{L/C_P}\ , \quad (3.7)$$

$$C(\eta,\xi)-C_\infty=C^0(\eta)-C_\infty=\frac{(C_b-C_\infty)E_1(p_C\eta)}{E_1(p_C)}\ . \quad (3.8)$$

The interface temperature and concentration, T_b and C_b, respectively, can now be determined by substituting Eqs. (3.6)—(3.8) in the two continuity relations Eqs. (3.4) and (3.5),

$$\frac{T_b-T_\infty}{L/c_p}=p_L E_1(p_L)e^{p_L}\ , \quad (3.9)$$

$$\frac{C_b-C_\infty}{C_b}=p_C E_1(p_C)e^{p_C}\ . \quad (3.10)$$

Finally, a single relation between Péclet number, effective undercooling, and solute concentration is obtained by substituting the above expressions for the interface temperature and concentration, Eqs. (3.9) and (3.10), in the Gibbs-Thomson relation [Eq. (3.2)],

$$\Delta_e=\frac{T_M-T_\infty}{L/c_p}-\beta C_\infty=p_L E_1(p_L)e^{p_L} +\frac{\beta C_\infty p_C E_1(p_C)e^{p_C}}{1-p_C E_1(p_C)e^{p_C}}\ . \quad (3.11)$$

This relation is the generalization of Eq. (2.2) for the pure thermal case to the case of dilute solutions and characterizes a family of tip radii and growth rates.

We now calculate how Eq. (3.11) is modified when capillary forces are included ($d_0\neq 0$). As we mentioned earlier in the Introduction, several authors in the past have made the assumption that the dendrite remains a perfect paraboloid when capillary forces are present and then compensated for this assumption by imposing the continuity relations (3.4) or (3.5) only at $\xi=0$. These calculations were carried out for a single diffusion field, thermal or chemical. However, in the present case, we have two coupled diffusion fields and accordingly two continuity relations (3.4) and (3.5). If we impose the two continuity conditions only at $\xi=0$, the problem we are left with is underconstrained in that there is not enough information to determine the diffusion fields uniquely. On the other hand, if we impose the two continuity conditions for all values of ξ, the problem is overconstrained in that the boundary conditions are not consistent with the assumption of a paraboloidal tip. In order to resolve this dilemma we note that both fields are diffusing away from the same interface and that consequently the velocity v, implicit in the Péclet numbers on the left-hand sides, is identical in Eqs. (3.4) and (3.5). If we eliminate this velocity between the two continuity conditions, we obtain an equality which must hold for all values of ξ,

$$\frac{1}{C(1,\xi)}\frac{\partial C}{\partial\eta}\bigg|_{\eta=1}=\frac{p_C}{p_L}\left[\beta^T\frac{\partial U_S}{\partial\eta}\bigg|_{\eta=1}-\frac{\partial U_L}{\partial\eta}\bigg|_{\eta=1}\right]\ . \quad (3.12)$$

This relation together with the Gibbs-Thomson relation (3.2) now allows us to determine the thermal and chemical fields everywhere in space. Then finally a single relation between Péclet number, effective undercooling, and solute concentration similar to Eq. (3.11) can be obtained by imposing any of the two equivalent continuity relations only at $\xi=0$. We emphasize that the two relations are now equivalent because we already have used Eq. (3.12) to determine the diffusion fields. We choose to impose the impurity conservation condition at $\xi=0$,

$$p_C C(1,0) = -\left.\frac{\partial C(\eta,0)}{\partial \eta}\right|_{\eta=1} . \tag{3.13}$$

In order to carry out the calculation analytically, we have to make two further approximations. The first approximation aims at removing a mathematical complication encountered in Eq. (3.12). In its present form this relation is nonlinear in the chemical field and cannot be used practically to determine the diffusion fields. However, to remove this difficulty, we can linearize Eq. (3.12) about the zeroth-order Ivantsov solutions. Typically the tip radius is several orders of magnitude larger than the capillary length, and, consequently, the concentration and temperature fields at the interface are not much different from the uniform Ivantsov results.

We define reduced fields $U_i'(\eta,\xi)$ and $C'(\eta,\xi)$ such that

$$U_i'(\eta,\xi) = U_i(\eta,\xi) - U_i^0(\eta),\ i=S,L$$
$$C'(\eta,\xi) = C(\eta,\xi) - C^0(\eta) .$$

Then we linearize (3.12) and obtain, after separating the ξ-dependent and ξ-independent parts of the equality, two relations:

$$\frac{1}{C_b}\left.\frac{\partial C^0}{\partial \eta}\right|_{\eta=1} = \frac{p_C}{p_L}\left.\frac{\partial U^0}{\partial \eta}\right|_{\eta=1} , \tag{3.14}$$

$$\frac{1}{C_b}\left.\frac{\partial C'(\eta,\xi)}{\partial \eta}\right|_{\eta=1} - \frac{C'(1,\xi)}{C_b^2}\left.\frac{\partial C^0}{\partial \eta}\right|_{\eta=1} = \frac{p_C}{p_L}\left[\left.\frac{\partial U_L'}{\partial \eta}\right|_{\eta=1} - \beta^T \left.\frac{\partial U_S'}{\partial \eta}\right|_{\eta=1}\right] . \tag{3.15}$$

We note that the separation of Eq. (3.12) into ξ-dependent and ξ-independent parts is possible here because the capillary corrections vanish as $\xi \to \infty$ and therefore (3.14) and (3.15) must hold independently. Equation (3.15) is linear in the reduced diffusion fields and can be used straightforwardly with Eq. (3.2) to determine these fields. When expressed in terms of the reduced fields and, again, after separating the ξ-dependent and ξ-independent parts of the equality, Eq. (3.2) becomes

$$\left[\frac{T_b - T_\infty}{L/C_p}\right] + \beta(C_b - C_\infty) = \Delta_e , \tag{3.16}$$

$$U_L'(1,\xi) + \beta C'(1,\xi) = -\frac{d_0}{\rho}\left[\frac{2+\xi}{(1+\xi)^{3/2}}\right] . \tag{3.17}$$

A second approximation, identical to one made by Kotler and Tarshis[10] for the pure thermal case, is that we neglect the term $p\xi$ in the diffusion equations (3.2). Our reason for doing this is that it allows us to write both the U and C fields as Fourier-Bessel transforms with compatible arguments involving the variable ξ, and thus we are able to construct explicit solutions for Eqs. (3.15) and (3.17) where the two fields are coupled. This approximation might lead to significant errors, especially because the chemical Péclet number p_C tends not to be much smaller than unity in these calculations. On the other hand, we shall use the results of this calculation only at $\xi=0$, where the error might not be so serious. Short of resorting to a very much harder numerical procedure, however, we have not been able so far to estimate the accuracy of this approximation, and simply must list it as another source of uncertainty. The diffusion equations now have the form

$$\left[\eta\frac{\partial^2}{\partial \eta^2} + (1+\eta p)\frac{\partial}{\partial \eta} + \xi\frac{\partial^2}{\partial \xi^2} + \frac{\partial}{\partial \xi}\right]\Xi(\eta,\xi) = 0 , \tag{3.18}$$

where p and Ξ are defined as before.

The calculation now proceeds as follows. First we solve the modified diffusion equation (3.18) by separation of variables and express the reduced diffusion fields as superpositions of special functions. Next we impose the two linear boundary conditions (3.17) and (3.15) together with the continuity of temperature across the interface to determine the diffusion fields everywhere in space. Then we impose the continuity equation (3.13) at $\xi=0$ and obtain a single relation between the following quantities: βC_∞, p_L, p_S, p_C, and C_b. Finally, we express C_b as a function of Δ_e, βC_∞, p_C, and p_L via Eqs. (3.14) and (3.16) and we obtain a single relation between Δ_e, βC_∞, p_L, p_S, and p_C.

The details of the calculation are rather technical and are shown in the Appendix. We quote only the final result

$$p_L E_1(p_L) e^{p_L} + \frac{\beta C_\infty p_C E_1(p_C) e^{p_C}}{1 - p_C E_1(p_C) e^{p_C}} = \Delta_e - \frac{2\alpha d_0}{\rho^2 \nu}\delta , \tag{3.19}$$

where δ is a complicated function of p_C, p_L, etc., given by Eq. (A10). The quantity $2\alpha d_0/\rho^2\nu = \sigma^*(C_\infty)$ is a dimensionless parameter which characterizes the point of marginal stability and will be calculated in Sec. IV. A comparison of Eqs. (3.11) and (3.19) shows that the effect of capillary forces is to reduce the effective undercooling and consequently to decrease the dendritic growth rate and enlarge the tip radius.

IV. STABILITY THEORY WITH IMPURITIES

Let us now look at the stability of the needle tip when impurities are present in the melt. Before going into a detailed quantitative calculation, we can first understand qualitatively the effect of impurities on the stability of the dendritic tip. The stability length λ_s defined in Eq. (2.5) is the geometric mean of the thermal capillary length d_0 and the thermal diffusion length $l_T = 2\alpha/\nu$ which characterizes the thickness of the layer of warm fluid ahead of the solidifying interface. When impurities are added to the melt there will also be an impurity-rich layer of thickness $l_C = 2D/\nu$. This impurity layer may destabilize the interface on a length scale which is smaller than λ_s by the ratio $\sqrt{D/\alpha}$, thus leading to sharper and faster dendritic structures.

We now make this argument quantitative by extending the stability analysis of Mullins and Sekerka[13] for a growing sphere to a situation where two coupled diffusion fields are present. We approximate the tip of the dendrite by a sphere of radius ρ growing at radial velocity v in an

undercooled melt and then we calculate the amplification rate for a perturbation proportional to the spherical harmonic l,m. For convenience we define the following reduced fields:

$$\delta U_i(r,\Theta,\varphi)=\frac{T(r,\Theta,\varphi)-T_M(C_\infty)}{L/c_P},\quad i=L,S$$

$$\delta C(r,\Theta,\varphi)=C(r,\Theta,\varphi)-C_\infty ,$$

where r is the radial distance from the center of the sphere, Θ and φ are the polar angles, and $T_M(C_\infty)$ is the melting temperature for a solution of concentration C_∞ (Fig. 2). Again the reduced fields satisfy four boundary conditions at the interface.

(1) Gibbs-Thomson relation:

$$\delta U_i \mid_{\text{int}}+\beta\delta C \mid_{\text{int}}=-d_0 K \mid_{\text{int}},\quad i=L,S . \tag{4.1}$$

(2) Continuity of temperature at the interface:

$$\delta U_s \mid_{\text{int}}=\delta U_L \mid_{\text{int}} . \tag{4.2}$$

(3) Conservation of impurities:

$$C \mid_{\text{int}} v_n=-D\vec{\nabla}(\delta C)\cdot\vec{n} \mid_{\text{int}} . \tag{4.3}$$

(4) Heat conservation:

$$v_n=-\alpha(\vec{\nabla}\delta U_L-\beta^T\vec{\nabla}\delta U_S)\cdot\vec{n} \mid_{\text{int}} . \tag{4.4}$$

Next we consider a slightly deformed sphere whose radius R is given in terms of spherical coordinates Θ and φ by $R=\rho+\delta_l Y_{lm}(\Theta,\varphi)e^{\omega_l t}$, where δ_l is small and $Y_{lm}(\Theta,\varphi)$ is the spherical harmonic of order l,m. Associated with this deformation are diffusion fields of the form

$$\delta U_i(r,\Theta,\varphi)=\delta U_i^0(r)+\delta U_i'(r)Y_{lm}(\Theta,\varphi)e^{\omega_l t},\quad i=L,S$$

$$\delta C(r,\Theta,\varphi)=\delta C^0(r)+\delta C'(r)Y_{lm}(\Theta,\varphi)e^{\omega_l t} ,$$

where δU_i^0 and δC^0 are the diffusion fields for the undeformed sphere and $\delta U_i'(r)$ and $\delta C'(r)$ are the response to the small amplitude deformation. In a quasistationary approximation, $\delta U_i'(r)$ and $\delta C'(r)$ satisfy Laplace's equation and are of the form

$$\delta U_L'(r)=a_l/r^{l+1} ,$$

$$\delta U_S'(r)=b_l r^l ,$$

$$\delta C'(r)=\hat{a}_l/r^{l+1} .$$

We can now determine a_l, b_l, $\hat{a}_l$, and the amplification rate ω_l by imposing the four boundary conditions [Eqs. (4.1)—(4.4)] on the reduced diffusion fields at the interface $r=R$, and then by linearizing the four independent relations. We list these four linearized relations below in the same order as Eqs. (4.1)—(4.4):

$$-\frac{\nu\delta_l}{\alpha}+\frac{a_l}{\rho^{l+1}}-\frac{\beta\nu C_b\delta_l}{D}+\frac{\beta\hat{a}_l}{\rho^{l+1}}=-d_0\frac{(l-1)(l+2)\delta_l}{\rho^2} , \tag{4.5}$$

$$-\frac{\nu\delta_l}{\alpha}+\frac{a_l}{\rho^{l+1}}=b_l\rho^l , \tag{4.6}$$

$$C_b\omega_l\delta_l-\frac{\nu^2 C_b\delta_l}{D}+\frac{\hat{a}_l\nu}{\rho^{l+1}}=-\frac{2\nu C_b\delta_l}{\rho}+\frac{D(l+1)\hat{a}_l}{\rho^{l+2}} , \tag{4.7}$$

$$\omega_l\delta_l=-\frac{2\nu\delta_l}{\rho}+\frac{\alpha a_l(l+1)}{\rho^{l+2}}+\beta^T\alpha l b_l\rho^{l-1} . \tag{4.8}$$

It is then straightforward to solve for the amplification rate ω_l and identify the point of marginal stability ($\omega_l=0$). Let $\sigma^*(0)$ denote σ^* for a pure substance as given by Eq. (2.10) and let $\sigma^*(C_\infty)$ be the value of σ^* at concentration C_∞. We obtain

$$\frac{\sigma^*(C_\infty)}{\sigma^*(0)}=1+\frac{\beta C_\infty(\alpha/D)}{1-p_C E_1(p_C)e^{p_C}}\times\left[1+\beta^T\left[\frac{l}{l+1}\right]\right]\left[\frac{1}{1-\frac{2p_C}{l+1}}\right] . \tag{4.9}$$

V. DISCUSSION

As seen in the preceding calculations, the behavior of the dendritic system is determined by two competing impurity effects. On one hand, the slowly diffusing impurities retard the growth of the solid, and on the other hand, the impurities destabilize the interface on a smaller length scale than the thermal-stability length, therefore sharpening the dendritic tip and enhancing the growth rate. The first of these effects is contained in Eq. (3.11) or (3.19). Typically D is much smaller than α and consequently $p_C=(\alpha/D)p_L$ is large. It then follows from Eq. (3.11) or (3.19) that one needs to impose a large Δ_e in order to maintain a constant value of p_L. Equivalently, at a constant undercooling Δ_e, an addition of impurities will reduce the value of p_L and therefore will tend to reduce the growth rate via Eq. (2.7).

The second of these effects is contained in Eq. (4.9). The enhanced value of σ^* with solute concentration implies an increase in dendritic growth rate via Eq. (2.7) and a decrease in tip radius via Eq. (2.8). At small impurity concentration the stability effect will be dominant and the tip velocity will be enhanced. As the impurity concentration is increased further the effect of the slow chemical diffusion will be dominant and the tip velocity will decrease after reaching a maximum.

Recent experiments on dendritic growth in dilute alloys have been carried out by Glicksman and Chopra[8] for solutions of acetone and argon in succinonitrile ($CN\text{-}C_2H_4\text{-}NC$). We concentrate here on the acetone-succinonitrile system where the experiments have been done for a larger range of solute concentration than for the argon-succinonitrile system. For acetone in succinonitrile the ratio of the thermal to chemical diffusion constant $\alpha/D\cong 91.3$. A comparison between experimental and theoretical results for V, $\tilde{\rho}$, and $\sigma^*(C_\infty)/\sigma^*(0)$ as functions of βC_∞ are shown in Figs. 4, 5, and 6, respectively, for an undercooling of 0.5 °C ($\Delta_e=0.022$). The solid line and the dashed line are obtained by combining Eqs. (4.9), (2.7), and (2.8) with Eqs. (3.11) and (3.19), respectively.

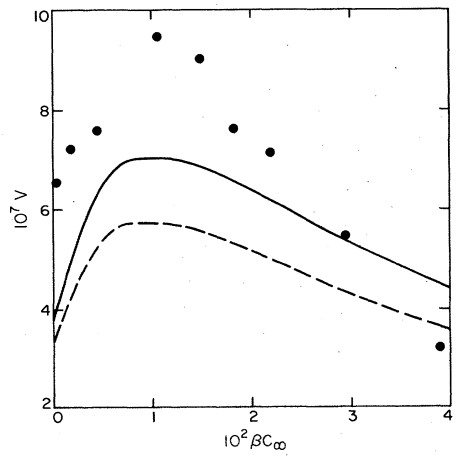

FIG. 4. Dimensionless velocity V vs dimensionless solute concentration βC_∞ for the acetone-succinonitrile system. Theoretical results with and without the capillary corrections are indicated by a dashed line and a solid line, respectively.

The dashed line corresponds to the theory where capillary forces are included and the solid line where they are neglected. The experimental data of Glicksman and Chopra are indicated by circles. It is apparent that both V and $\tilde{\rho}$ exhibit velocity enhancement and tip sharpening, respectively, at small impurity concentration and that both of these effects have the right order of magnitude. We also note a good agreement with experiment for the stability parameter $\sigma^*(C_\infty)$ at small impurity concentration. The quantitative discrepancies for both $\tilde{\rho}$ and V can be attributed partly to convective effects. Going back to Fig. 1 we observe for pure succinonitrile a systematic deviation of the experimentally observed tip velocity from the results of the purely diffusion-controlled theory at small undercooling. In the present case the undercooling of 0.5 °C is well within the region where convective effects become important. A more serious discrepancy, however, is the deviation of $\sigma^*(C_\infty)/\sigma^*(0)$ at solute concentration

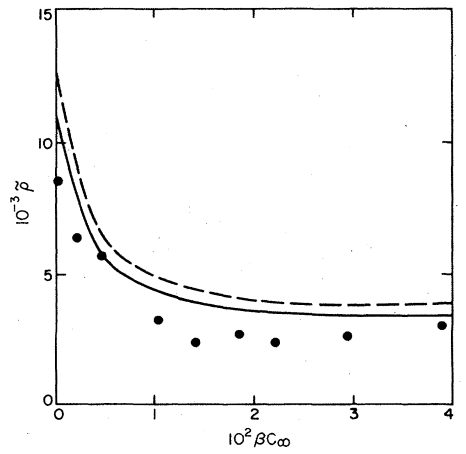

FIG. 5. Dimensionless tip radius $\tilde{\rho}$ vs dimensionless solute concentration βC_∞ for the acetone-succinonitrile system. Theoretical results with and without the capillary corrections are indicated by a dashed line and solid line, respectively.

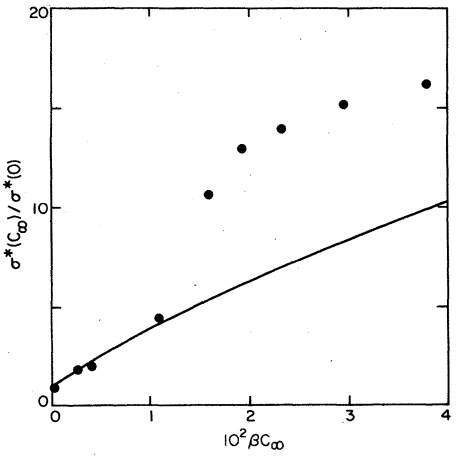

FIG. 6. Stability parameter $\sigma^*(C_\infty)/\sigma^*(0)$ vs dimensionless solute concentration βC_∞.

beyond the maximum velocity point ($\beta C_\infty > 10^{-2}$). We note that a similar discrepancy has been observed for the argon-succinonitrile system but, in the opposite direction, the experimental values were below the theoretical prediction of Eq. (4.9) for solute concentration larger than the point of maximum velocity. These deviations cannot be easily attributed to convection effects because the stability of the needle tip depends mainly on a thin boundary layer of impurities which is for the most part unaffected by convective transport. However, these discrepancies could possibly be explained by a breakdown of the spherical approximation in the stability analysis. The experiments show a change in dendritic morphology at small impurity concentration. The sidebranches move up toward the tip as the concentration is increased initially and then recede backwards along the dendrite when the concentration is increased further past the point of maximum velocity. This behavior suggests doing a more realistic stability analysis of the dendritic tip.

In conclusion, we have described a theory of diffusion-controlled dendritic growth for dilute alloys. The theory predicts a velocity enhancement and a tip sharpening in qualitative agreement with experiments. However, only part of the quantitative discrepancies can be attributed to convective effects and deviations of the stability constant from experimental values at higher solute concentration suggest doing a more detailed stability analysis of the needle crystal.

ACKNOWLEDGMENTS

This research was supported by Department of Energy Contract No. DE-AM03-76SF00034 and, in part, by the National Science Foundation under Grant No. PHY-77-27084, supplemented by funds from the U.S. National Aeronautics and Space Administration.

APPENDIX

Let $\Xi(\eta,\xi)=A(\eta)B(\xi)$ be a solution of Eq. (3.18). Then (3.18) separates into independent equations for each of the parabolic coordinates

$$\eta\frac{\partial^2}{\partial\eta^2}A+(1+\eta p)\frac{\partial A}{\partial\eta}=\frac{\lambda^2}{4}A\ , \tag{A1}$$

$$\xi\frac{\partial^2 B}{\partial\xi^2}+\frac{\partial B}{\partial\xi}=-\frac{\lambda^2}{4}B\ , \tag{A2}$$

where λ^2 is the separation constant. The solutions to Eqs. (A1) and (A2) can be expressed in terms of the zeroth-order Bessel function and confluent hypergeometric functions

$$B(\xi)=J_0(\lambda\sqrt{\xi})\ ,$$

$$A(\eta)=\begin{cases}\varphi(-\lambda^2/4p,1,-\eta p), & \eta<1 \text{ (solid)}\\ e^{-p\eta}\psi(1+\lambda^2/4p,1,p\eta), & \eta>1 \text{ (liquid)}\end{cases}$$

where φ and ψ are the confluent hypergeometric functions of the first kind and the second kind, respectively.[17]

A general solution of Eq. (3.18) can be expressed as a superposition of special functions, and we can write the reduced diffusion fields in the following way:

$$U_S'(\eta,\xi)=\int_0^\infty f(\lambda)J_0(\lambda\sqrt{\xi})\times\frac{\varphi(-\lambda^2/4p_S,1,-\eta p_S)}{\varphi(-\lambda^2/4p_S,1,-p_S)}\ , \tag{A3}$$

$$U_L'(\eta,\xi)=\int_0^\infty f(\lambda)J_0(\lambda\sqrt{\xi})\times\frac{e^{-p_L\eta}\psi(1+\lambda^2/4p_L,1,p_L\eta)}{e^{-p_L}\psi(1+\lambda^2/4p_L,1,p_L)}\ , \tag{A4}$$

$$C'(\eta,\xi)=\int_0^\infty g(\lambda)J_0(\lambda\sqrt{\xi})\times\frac{e^{-p_C\eta}\psi(1+\lambda^2/4p_C,1,p_C\eta)}{e^{-p_C}\psi(1+\lambda^2/4p_C,1,p_C)}\ . \tag{A5}$$

The fact that the same distribution function $f(\lambda)$ appears in both (A3) and (A4) follows from the continuity of temperature at the interface. Next we impose Eqs. (3.15) and (3.17) and obtain two simultaneous equations for $f(\lambda)$ and $g(\lambda)$:

$$-\frac{p_C}{C_b}\frac{\psi(1+\lambda^2/4p_C,2,p_C)g(\lambda)}{\psi(1+\lambda^2/4p_C,1,p_C)}+\frac{g(\lambda)}{C_b^2}\frac{(C_b-C_\infty)}{E_1(p_C)e^{p_C}}=-p_C\frac{\psi(1+\lambda^2/4p_L,2,p_L)}{\psi(1+\lambda^2/4p_L,1,p_L)}f(\lambda)-(p_C/p_L)\beta^T\frac{\lambda^2}{4}\frac{\varphi(1-\lambda^2/4p_S,2-p_S)}{\varphi(-\lambda^2/4p_S,1,-p_S)}f(\lambda)\ , \tag{A6}$$

$$f(\lambda)+\beta g(\lambda)=-\frac{d_0}{\rho}e^{-\lambda}(1+\lambda)\ . \tag{A7}$$

We impose Eq. (3.13) at $\xi=0$:

$$1=\frac{C_b-C_\infty}{C_bE_1(p_C)e^{p_C}p_C}+\int_0^\infty d\lambda\frac{g(\lambda}{C_b}\left[\frac{\psi(1+\lambda^2/4p_C,2,p_C)}{\psi(1+\lambda^2/4p_C,1,p_C)}-1\right]\ . \tag{A8}$$

Combining Eqs. (3.16) and (3.14) we obtain one more relation,

$$\frac{E_1(p_L)e^{p_L}p_L}{E_1(p_C)e^{p_C}p_C}\left[\frac{C_b-C_\infty}{C_b}\right]+\beta(C_b-C_\infty)=\Delta_e\ . \tag{A9}$$

We now have a complete solution to the problem. Combining (A6) and (A7) we solve for $g(\lambda)$ and substitute the answer into Eq. (A8). Finally, combining (A8) and (A9), we can eliminate C_b and obtain a single relation between Δ_e, βC_∞, and the Péclet numbers. The final result is shown in Eq. (3.19) where

$$\delta=\left[p_LE_1(p_L)e^{p_L}+\frac{\beta C_\infty p_CE_1(p_C)e^{p_C}}{(1-p_CE_1(p_C)e^{p_C})^2}\right]\times\int_0^\infty d\lambda e^{-\lambda}(1+\lambda)p_C\left[p_L\frac{\psi(1+\lambda^2/4p_L,2,p_L)}{\psi(1+\lambda^2/4p_L,1,p_L)}+\beta_T\frac{\lambda^2}{4}\frac{\varphi(1-\lambda^2/4p_S,2,-p_S)}{\varphi(-\lambda^2/4p_S,1,-p_S)}\right]$$

$$\times\left[\frac{\psi(1+\lambda^2/4p_C,2,p_C)}{\psi(1+\lambda^2/4p_C,1,p_C)}-1\right]\Bigg/\left[\frac{\beta C_\infty(p_C/p_L)}{1-p_CE_1(p_C)e^{p_C}}\left[\frac{p_L\psi(1+\lambda^2/4p_L,2,p_L)}{\psi(1+\lambda^2/4p_L,1,p_L)}+\beta_T\frac{\lambda^2}{4}\frac{\varphi(1-\lambda^2/4p_S,2,-p_S)}{\varphi(-\lambda^2/4p_S,1,-p_S)}\right]+\frac{p_C\psi(1+\lambda^2/4p_C,2,p_C)}{\psi(1+\lambda^2/4p_C,1,p_C)}-p_C\right]\ . \tag{A10}$$

It is important to mention that when we solve for δ [Eq. (A10)] we only keep first-order terms in the small parameter $2\alpha d_0/\rho^2\nu$. This is consistent with the linearization of Eq. (3.12) discussed earlier in Sec. II. Typically $2\alpha d_0/\rho^2\nu\sim[10^{-2},10^{-1}]$ and higher-order corrections will be very small.

[1]J. S. Langer and H. Müller-Krumbhaar, Acta Metall. **26**, 1681 (1978).
[2]J. S. Langer, Rev. Mod. Phys. 1, 52 (1980).
[3]G. Dee and J. S. Langer, Phys. Rev. Lett. **50**, 383 (1983).
[4]E. Ben-Jacob, N. Goldenfeld, J. S. Langer, and G. Schön, Phys. Rev. A **29**, 330 (1984).
[5]J. S. Langer, Physiochemical Hydrodynamics **1**, 41 (1980).
[6]T. Fujioka, Ph.D. thesis, Carnegie-Mellon University, 1978.
[7]C. Lindenmeyer, Ph.D. thesis, Harvard University, 1959.
[8]M. Glicksman (private communication); M. A. Chopra, Ph.D. thesis, Rensselaer Polytechnic Institute, 1983.
[9]D. E. Temkin, Dokl. Akad. Nauk SSSR **132**, 1307 (1960) [Sov. Phys.—Dokl. **5**, 609 (1960)].
[10]G. Kotler and L. Tarshis, J. Cryst. Growth **5**, 90 (1969).
[11]R. Trivedi, Acta Metall. **18**, 287 (1970).
[12]R. Sekerka, R. Seidensticker, D. Hamilton, and J. Harrison, Westinghouse Research Laboratory Report, 1967.
[13]W. Mullins and R. Sekerka, J. Appl. Phys. **34**, 323 (1963).
[14]H. Müller-Krumbhaar and J. S. Langer, Acta Metall. **29**, 145 (1981).
[15]M. Glicksman, R. Schaefer, and J. Ayers, Metall. Trans. **7A**, 1747 (1976).
[16]S. Huang and M. Glicksman, Acta Metall. **29**, 701 (1981).
[17]L. J. Slater, *Confluent Hypergeometric Functions* (Cambridge University, Cambridge, England, 1960).